Nuclear Instruments and Methods in Physics Research A 693 (2012) 226–235

Contents lists available at SciVerse ScienceDirect

Nuclear Instruments and Methods in Physics Research A

journal homepage: www.elsevier.com/locate/nima

Performance of thin long scintillator strips of GSO:Ce, LGSO:Ce and LuAG:Pr for low energy γ-rays

Masaaki Kobayashi [a,*], Souichiro Aogaki [b], Fujio Takeutchi [b], Yoichi Tamagawa [c], Yoshiyuki Usuki [d]

[a] IPNS, High Energy Accelerator Research Organization (KEK), Tsukuba 305-0801, Japan
[b] Faculty of Science, Kyoto Sangyo University, Kyoto 603-8555, Japan
[c] Graduate School of Engineering, University of Fukui, Fukui 910-8507, Japan
[d] Materials Research Laboratory, Furukawa Co. Ltd., Tsukuba 305-0856, Japan

ARTICLE INFO

Article history:
Received 19 June 2012
Received in revised form
16 July 2012
Accepted 21 July 2012
Available online 2 August 2012

Keywords:
Particle detector
GSO:Ce
LGSO:Ce
LuAG:Pr
Scintillator
Resolution
Single crystalline fibers
PET

ABSTRACT

Interest in fibers or strips of single crystalline scintillators is increasing for their possible applications in fine-segmented particle detectors for particle physics experiments as well as γ-ray detectors for medical diagnoses. We compared $2\times2\times100$ mm^3 strips of Gd_2SiO_5(GSO):Ce, $Lu_{1.9}Gd_{0.1}SiO_5$ (LGSO):Ce, and $Lu_3Al_5O_{12}$(LuAG):Pr single crystals for 0.511 MeV γ-rays with respect to the effective light attenuation length λ_a, light yield LY, FWHM energy resolution $\Delta E/E$ and rms position resolution $\sigma(z)$ of the injection position z along the length. The obtained result was (λ_a, LY, $\Delta E/E$, $\sigma(z)$)=(128 mm, 380 phe/MeV, 17.7%, 8.7 mm) in GSO:Ce, (509 mm, 1760 phe/MeV, 12.2%, 10.9 mm) in LGSO:Ce, and (171 mm, 690 phe/MeV, 15.0%, 8.9 mm) in LuAG:Pr. The z position was obtained independently from the pulse height ratio as well as the timing difference between both ends of the strip. The latter method gave comparable or even smaller $\sigma(z)$ than the former only in LGSO:Ce having both large LY and fast rise time. The λ_a in the 100 mm long GSO:Ce strip was found to be twice as large as that in the 200 mm long one [1] with the same cross-section. To obtain good $\Delta E/E$ and $\sigma(z)$, large light yield, fast rise time, and moderately large attenuation length are important for the scintillators.

1. Introduction

Single crystalline scintillators in fibers or strips have attracted increasing interest in these years [1–3] for their possible applications in fine-segmented detectors in particle physics [1,3] and γ-ray detectors in medical diagnoses [1,4,5]. In most of the applications, high-quality fibers or strips as long as 100–200 mm are required. Several scintillator strips were evaluated in the past, including $3.2\times3.2\times100$ mm^3 $(Lu,Y)_2SiO_5$(LYSO):Ce and $YAlO_3$(YAP):Ce [6], $3\times3\times100$ mm^3 LYSO:Ce [5], $1\times1\times43$ mm^3 and 1 mm diameter, 69 mm length LYSO:Ce [4], and $2\times2\times200$ mm^3 GSO:Ce [1].

In our previous work [1], we evaluated a $2\times2\times200$ mm^3 GSO:Ce 1.5 mol% strip for 0.511 MeV γ-rays. Employing photomultiplier tube (PMT) readout at both ends, we obtained the effective attenuation length λ_a=67 mm, FWHM energy resolution $\Delta E/E$=35–24% depending on the longitudinal position z, and the rms position resolution $\sigma(z)\sim10$ mm almost independently of z. While GSO:Ce should be promising, there may be better materials for fibers among heavy, fast response, and efficient scintillators.

With this motivation, we compared in the present work GSO:Ce, LGSO:Ce and LuAG:Pr, all having the same size of $2\times2\times100$ mm^3. The scintillator characteristics of these materials are compared in Table 1. The reason why we chose GSO:Ce was mentioned in Ref. [1]. It is one of dense, fast-response, and efficient scintillators with good balance [7,8], and has been widely used in particle detectors [9–11]. Its light yield (LY), however, is not large enough compared with some other Ce-activated scintillators such as Lu_2SiO_5(LSO):Ce, LYSO:Ce, LGSO:Ce, etc. It is then interesting to evaluate scintillator strips with higher LYs.

As for LSO:Ce, the internal non-uniformity has mostly been solved [12]. To overcome the remaining instability completely in both crystal growth and properties of grown crystals, mixed crystals of LSO:Ce with small concentrations of Y_2SiO_5 (LYSO:Ce [13]) or GSO (LGSO:Ce [14,15]) have been successfully developed in these years. Since LYSO:Ce and LGSO:Ce have the same crystal structure without cleavage and similar scintillation properties, we chose LGSO:Ce for the present study. The crystal structure is of LSO:Ce type (monoclinic structure, C2/c space group) if Lu:Gd molar ratio is larger than 0.2:0.8 [16]. The present sample with Lu:Gd=0.95:0.05 is close to LSO:Ce in almost all aspects. Besides the main emission peak at 410 nm, an additional peak at 310 nm occupies 18% of the total LY (Fig. 1). This peak, coming from the 4f–4f spin-forbidden transitions of Gd^{3+}, remains because the

* Corresponding author. Tel.: +81 267242234; fax: +81 267242234.
E-mail address: masaaki.kobayashi@kek.jp (M. Kobayashi).

0168-9002/$ - see front matter © 2012 Elsevier B.V. All rights reserved.
http://dx.doi.org/10.1016/j.nima.2012.07.045

Table 1
Scintillation characteristics of some heavy, efficient and fast-response single crystals including GSO:Ce, LGSO:Ce and LuAG:Pr.

Scintillator	GSO:Ce^{3+} 1.5 mol%	LGSO:Ce^{3+} (Lu 95%)	LSO:Ce^{3+}	LuAG:Pr^{3+}	LuAG:Ce^{3+}	$Bi_4Ge_3O_{12}$ (BGO)
Density, g/cm^3	6.71	7.3	7.40	6.73	6.73	7.13
Radiation length cm	1.38	1.16	1.14	1.45	1.45	1.12
Effective atomic number Z_{eff}	59.4	66.1	66.4	62.9	62.9	75.2
Refractive index n[a]	1.85[b] [1]	1.83	1.83 [23]	1.99 [24]	1.84[c]	2.15 [25]
μ[d] at 511 keV, cm^{-1}	0.71	0.86	0.88	0.75	0.75	0.98
Emission peak, nm	430	410	410	310, 365	520	480
Excitation peak, nm	310, 350	380	380	240, 280	470	280
LY[e], phe/MeV	8000[f]	23,000	27,000	18,000	18,000	8000
Decay constant τ, ns	28 (87%)[f], 260 (13%)[f]	40	40	17 (35%), 119 (14%), 1600	69 (40%) 1500	300
10–90% rise time t_{rise}, ns	8[f]	~1	~1	0.41		<0.1
References	[1,7,8,17]	[18]	[8,19]	[20,21]	[21]	[22]

[a] n is given at the emission peak wavelength unless otherwise indicated.
[b] Values at 633 nm or average for standard daylight.
[c] At Na-D line (589.3 nm).
[d] μ at 511 keV=absorption coefficient for γ-rays at 0.511 MeV.
[e] LY=light yield obtained in pulse measurement within ~1 μs gate; much slower components than ~μs are ignored.
[f] For the standard Ce concentration of 0.5 mol%, LY=10,000 phe/MeV [1]; τ=53 ns(90%), 400 ns(10%); t_{rise}=13 ns [17].

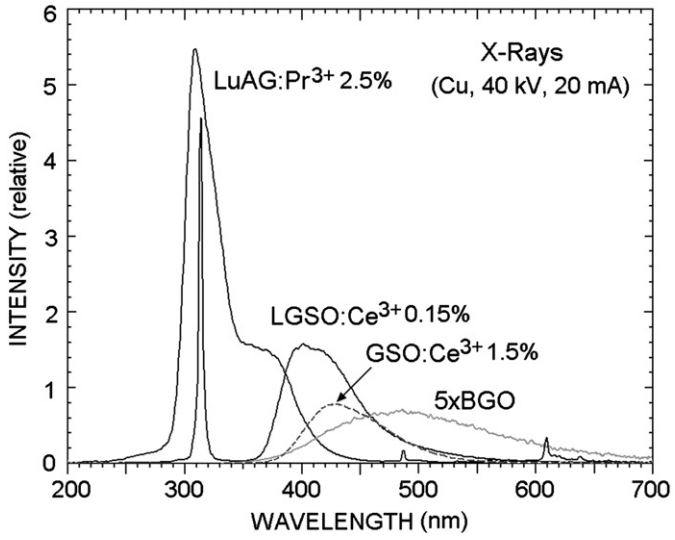

Fig. 1. Radioluminescence spectra of GSO:Ce1.5 mol% ($20\times20\times200$ cm^3), LGSO:Ce0.15 mol% ($1\times1\times1$ cm^3) and LuAG:Pr2.5 mol% ($5\times30\times3$ mm^3) single crystals for X-rays. Sharp peaks of LuAG:Pr^{3+} above 480 nm should be due to 4f–4f radiative transitions of Pr^{3+}.

Gd–Gd energy migration to Ce^{3+} should be weak due to small concentration of Gd^{3+}. Since the 310 nm component should be slow enough with a decay constant τ~ms, its existence should hardly disturb the present measurement.

We also included LuAG:Pr^{3+} for the present study. Compared with GSO:Ce, it has a similar density, a little larger Z_{eff} (62.9 compared to 59.4), and rather different scintillation properties (Table 1). The emission peak sits at 310 nm, much shorter wavelength than GSO:Ce (Fig. 1). It fits well the UBA (ultra bialkali) or SBA (super bialkali) photocathode PMTs [26], which have the maximum quantum efficiency (QE) around 350 nm. The total LY is large between GSO:Ce and LGSO:Ce. The decay has a fast component of τ=17 ns (for 35% in intensity) and medium one of 119 ns (14%). The fast component is roughly similar to GSO:Ce in intensity, but much faster. The 10–90% rise time of 0.4 ns [20] is much faster than 8 ns in GSO:Ce (Table 1).

One of the interests in the present study lies in λ_a. Although LGSO:Ce, and LuAG:Pr have much larger LY than GSO:Ce, the overlap of the excitation and emission spectra in the tails is as large as or even larger than in GSO:Ce (see Fig. 2). Self-absorption may limit the obtainable LYs in the strips.

All the single crystalline strips studied in the present work were cut from Czochralski-grown ingots of high quality. Since single crystalline fibers commercially available are limited in materials as well as size, it was not easy to get fiber samples of a fixed size with the scintillation properties as good as bulk single crystals.

Production of single crystalline fibers has been developed [2] with several methods including (1) micro-pulling-down (μPD), (2) edge defined film-fed growth (EFG), (3) laser-heated pedestal growth (LHPG), and (4) internal crystallization method (ICM). Among them, μPD method has been expected to be promising in growing long fibers at a reasonable cost. To the authors' knowledge, GSO:Ce fibers of the present length (100 mm) have not yet been realized. This may be related to the cleavage of this crystal. LGSO:Ce fibers are not yet available, differently from LYSO:Ce. In a pioneering work for a small PET (positron emission computed tomography) scanner [4], LYSO fibers with a cross-section of about 1 mm^2 and a length of 70 mm were grown by the μPD method, and evaluated with respect to the scintillation properties. A clear LSO:Ce fiber of 0.5 mm diameter and 20 mm length [27] was also grown with the LHPG method. The situation as mentioned above may indicate a possibility of growing LGSO:Ce fiber in the near future.

In contrast to GSO:Ce and LGSO:Ce, LuAG:Pr fibers have already been grown successfully at a few laboratories and companies [28,3]. In Furukawa Co., one of the present authors (Y.U.) has successfully grown single crystal fibers of LuAG:Pr 2.5 mol% longer than 200 mm with a cross-section of 2×2 mm^2 by the μPD method. The grown fiber was clear with the cross-section uniform. However, we had some difficulty in cutting both ends at a precise length; small cracking occurred probably due to the stress remaining in the crystal even after annealing. The reason why this difficulty does not occur in LuAG:Ce fiber but in LuAG:Pr remains to be clarified in the future. For the present experiment, we abandoned crystal fiber of LuAG:Pr, and cut the strip from a Czochralski-grown ingot.

For most of the applications mentioned above, the energy deposit of injected particle in a strip should be as small as a few MeV. We therefore evaluated each crystal strip for 0.511 MeV γ-rays, which can be easily obtained from the back-to-back annihilation of a positron from ^{22}Na on an electron. A narrow γ-ray beam can be obtained by a tagging technique [1,29].

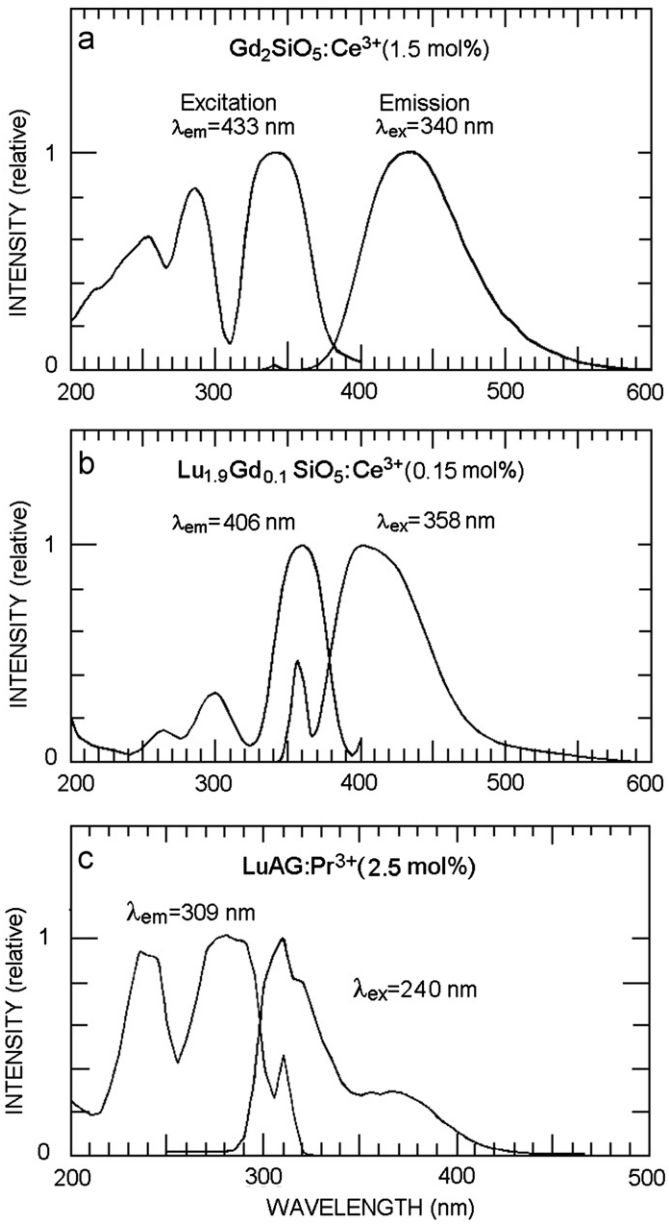

Fig. 2. Excitation and emission spectra of (a) GSO:Ce, (b) LGSO:Ce and (c) LuAG:Pr. For the sample size, see the captions of Fig. 1. The overlap between the excitation and emission spectra in the tails are larger in LGSO:Ce and LuAG:Pr than in GSO:Ce.

The main aim of the present paper is to compare λ_a, LY, $\Delta E/E$, and $\sigma(z)$ for the three crystals. After description of the measuring method in the next section, the obtained results are given in Section 3. Section 4 is devoted to discussions on λ_a, LY, energy and position resolutions before coming to a summary in Section 5.

2. Experimental

A GSO:Ce 1.5 mol% strip with $2\times2\times100$ mm^3 was cut from a longer strip of $2\times2\times200$ mm^3, which came from the same ingot as the 200 mm long strip evaluated in Ref. [1]. The whole surface was polished to the optical grade by chemical etching. Compared with the standard Ce^{3+} concentration of 0.5 mol%, the present crystal should give 80% of light intensity [1], a shorter τ of 28 instead of 53 ns, and a faster rise time (10–90%) of 8 instead of 13 ns [17].

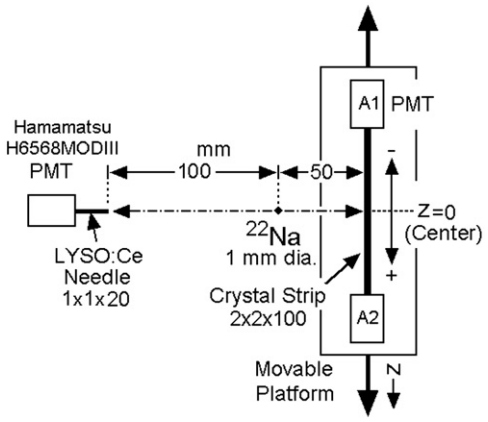

Fig. 3. A sketch of the setup. PMTs as well as their pulse heights on both ends of crystal strip are called $A1$ and $A2$. The distance z of the injection position of 0.511 MeV γ-rays on the strip measured from its center ($z=0$) increases from $-L/2$ at A1 toward $L/2$ at A2, here L being the strip length of 100 mm.

A single crystal of LGSO:Ce with a diameter of 50 mm was grown by Hitachi Chemical Co. with Lu:Gd molar ratio=0.95:0.05 and Ce^{3+} concentration of 0.15 mol % in the melt. A strip of $2\times2\times100$ mm^3 was cut from the ingot and polished by chemical etching.

A LuAG:Pr single crystal was grown by Furukawa Co. with the Czochralski method using an Ir crucible. The Pr^{3+} concentration was 2.5 mol% in the melt, while 0.2 mol% in the crystal. The small segregation coefficient of 0.062 should be due to the significant mismatch in the ion radii between Lu^{3+} (0.85 Å) and Pr^{3+} (1.06 Å). A strip of $2\times2\times100$ mm^3 was cut from the ingot and polished by chemical etching.

The experimental setup as sketched in Fig. 3 was placed in a light-shielded box. Each scintillator strip was directly coupled to a PMT on both ends (called $A1$ and $A2$) with optical grease Oken 6262. The strip without reflector wrapping nor coating was mechanically supported only by a 7 mm thick bakelite holder at each PMT window. For each PMT, one of the 16 anodes of position sensitive PMT (Hamamatsu H6568MODIII, UBA, QE=41% max at 350 nm, borosilicate glass window) was assigned. The fixed channels on the fixed PMTs were used for different scintillators by remounting them.

The 0.511 MeV γ-rays were injected to a small spot on the scintillator strip by using a tagged γ-ray injector [1]. The injector consists of a ^{22}Na γ-ray source (1 mm diameter) and a needle of $Lu_{1.96}Y_{0.04}SiO_5$(LYSO):Ce^{3+} scintillator with $1\times1\times20$ mm^3. Lu-rich LYSO:Ce [13] has similar scintillation characteristics as LSO:Ce (Table 1). Both the LYSO needle and the scintillator strip were placed at a distance of 100 and 50 mm, respectively, from the ^{22}Na source on the opposite side. Two γ-rays emitted back to back were detected by the needle and the scintillator strip in coincidence. The γ-ray beam profile on the strip was scanned with another $1\times1\times20$ mm^3 LYSO:Ce needle at the scintillator strip position. The obtained 1-dimensional distribution of the γ-rays gave a Gaussian shape of 0.68 mm rms.

The scintillator strip mounted on an optical stand was moved along the direction of its length, taken as z-axis, while the γ-ray injector was fixed in position. Referring to Fig. 3, z gives the γ-ray injection position along the z-axis, increasing from $A1$ to $A2$ with $z=0$ at the center.

We carried out measurement for seven injection points $z=-40$, -20, 0, 10, 20, 30, and 40 mm using standard NIM-CAMAC circuits. The outputs of the LYSO needle and the scintillator strip were first amplified in a preamplifier (KN2104, Kaizu-Works Co., gain~4), and fed to a charge-sensitive ADC (14 bit, Hoshin C009H) within a

Table 2
Summary of the obtained result for 0.511 MeV γ-ray injection at $z=0$. LY and $\Delta E/E$ are for the sum of $A1$ and $A2$. The 200 mm long GSO:Ce [1] is also added for comparison.

Scintillator strip	GSO:Ce	LGSO:Ce	LuAG:Pr	GSO:Ce[1]
Size, mm^3	$2\times2\times100$	$2\times2\times100$	$2\times2\times100$	$2\times2\times200$
Attenuation length λ_a, mm	128	509	171	67
Light yield LY, phe/MeV	380	1758	691	114
FWHM energy resolution, $\Delta E/E$	0.177	0.122	0.150	0.35
rms position resolution $\sigma(z)$, mm				
From $A1/A2$	8.9	16.8	10.0	10.0
From $T1-T2$	42	14.3	19.2	32
Combined	8.7	10.9	8.9	9.5

350 ns gate (300 ns net for integration). The ADC signals or light yields of the PMTs $A1$ and $A2$ are also called $A1$ and $A2$, respectively, throughout the present paper. The timings of the $A1$ (denoted as $T1$) and $A2$ ($T2$) were registered with a TDC (12 bit for 100 ns, Philips 7187) with respect to the LYSO as the start.

Data taking was done under a triggering condition of hits in the LYSO and at least "$A1$ or $A2$" (for GSO:Ce), or both "$A1$ and $A2$" (for LGSO:Ce and LuAG:Pr) in coincidence. "$A1$ or $A2$" and "$A1$ and $A2$" should not make any sizable differences in event selection, since the threshold in both $A1$ and $A2$ was set a little below the single photoelectron (phe) level.

The pulse height spectrum of the LYSO needle was similar to Ref. [1]. The 0.511 MeV total absorption peak with 16.5% FWHM occupied 34% of the total LY, and was well separated from the Compton-scattering plateau. We did not require the LYSO pulse height to be in the total absorption peak in triggering and data analysis because of the following reason: when the two γ-rays from ^{22}Na are detected by the LYSO needle and the scintillator strip, the reaction of Compton scattering or total absorption of one of the γ-rays in the former detector is irrelevant to the reaction of the other γ-ray in the latter.

3. Results

The obtained results on LY, λ_a, $\Delta E/E$ and $\sigma(z)$ from pulse height measurement are first given separately for three crystals in Sections 3.1–3.3. Then in Section 3.4, the timing difference $T1-T2$ as well as the calculated $\sigma(z)$ will be compared for all the crystals. Typical results obtained for the injection at $z=0$ are summarized in Table 2.

3.1. GSO:Ce strip

Pulse height spectrum of $A1$ (or $A2$) consists of 0.511 MeV total absorption peak and Compton-scattering plateau. While we followed similar data analysis as in our previous work [1], the analysis was simpler this time because the separation of the total absorption peak from the Compton tail was much better due to the shorter strip.

Since the PMT gain, including preamplifiers, may be different for $A1$ and $A2$, we first normalized both gains by injecting the γ-rays at the center ($z=0$), and comparing the total absorption peak channels. All the results are given after this left and right normalization and pedestal subtraction.

A typical pulse height spectrum of the sum of $A1$ and $A2$ obtained at $z=0$ is given in Fig. 4 in comparison with the other crystals.

Fig. 5a gives the z-dependences of the $A1$ (actually the peak of $A1$ pulse height spectrum), $A2$, $A1+A2$ and $\Delta E/E$. The dependence of $A2$ (or $A1$) on z can be fit well with a single exponential besides a constant factor

$$A1\sim\exp(-z/\lambda_a)\quad\text{and}\quad A2\sim\exp(z/\lambda_a) \tag{1}$$

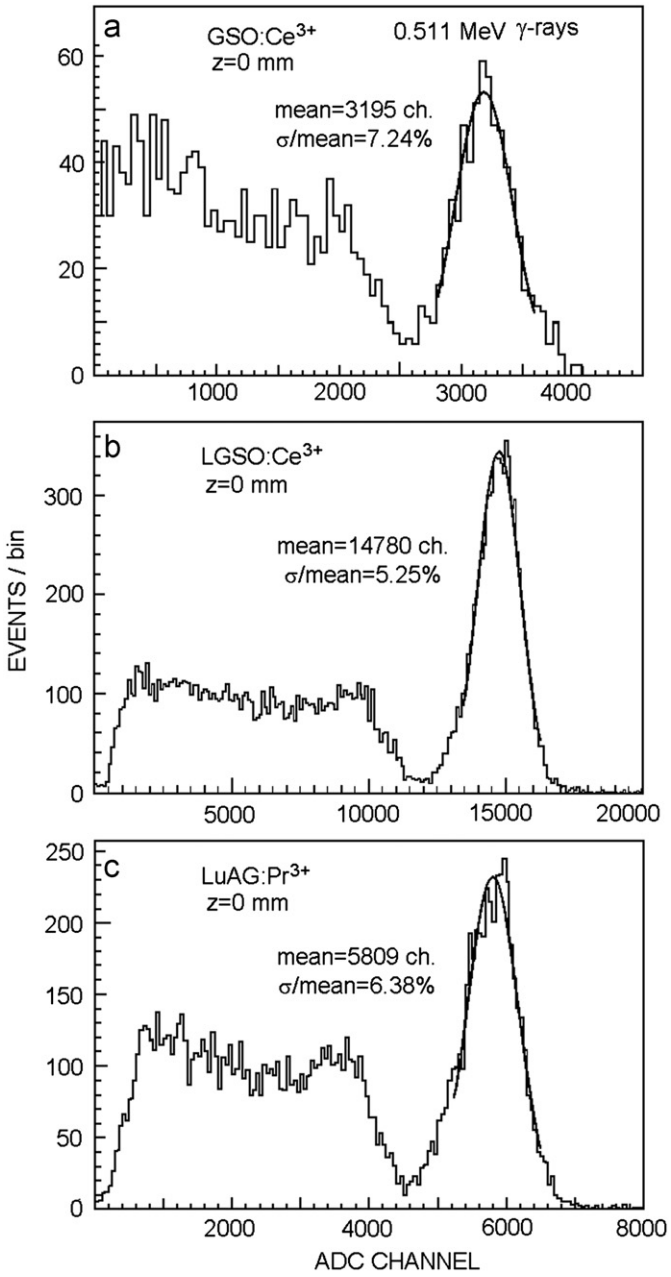

Fig. 4. Pulse height spectra of $A1+A2$ for 0.511 MeV γ-rays injected at $z=0$ in GSO:Ce, LGSO:Ce and LuAG:Pr strips under the triggering condition given in Section 2.2. The pedestal is already subtracted. Solid curve gives a Gaussian fit for the total absorption peak. Although the PMT high voltages (HVs) were 750, 700 and 720 V for GSO:Ce, LGSO:Ce and LuAG:Pr, respectively, so as to avoid saturation in PMT, the spectra are presented after gain normalization to the same HV. The bin width is 50 ch. in (a) and (c), while 100 ch. in (b).

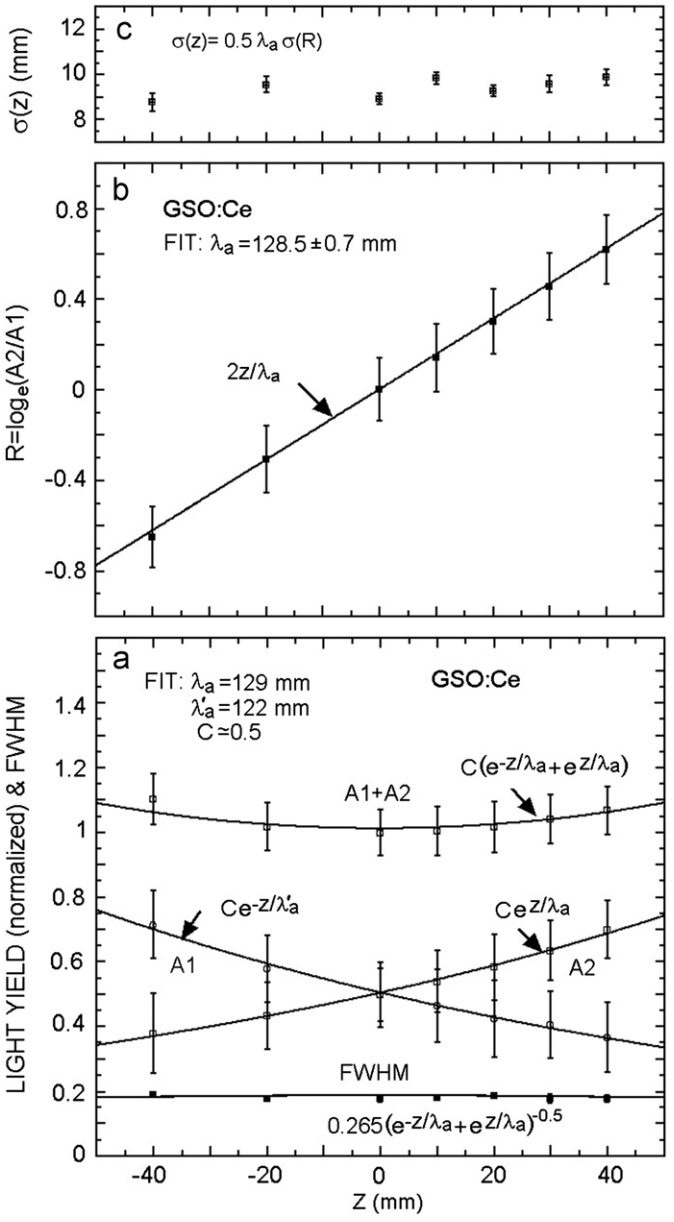

Fig. 5. Obtained result in GSO:Ce for 0.511 MeV γ-rays. See Section 2.2 for the triggering condition. (a) Pulse heights $A1$, $A2$, sum of $A1+A2$ and FWHM resolution of $A1+A2$ (also denoted as $\Delta E/E$ in text) versus longitudinal position z. (b) $R=\log_e(A2/A1)$, and (c) $\sigma(z)=\lambda_a\sigma(R)/2$ with $\sigma(R)$=rms width of the peak of R. In (a) and (b), solid curves give the fit (see text). In the fit for $A1+A2$ and FWHM, only the overall constant was taken as a fitting parameter by fixing λ_a at 129 mm (see text). The error bar attached to data points of any quantity Q=$A1$, $A2$, $A1+A2$ and R gives the rms width $\sigma(Q)$ of the Q (Gaussian) peak as typically seen in Fig. 4 for $Q=A1+A2$ and Fig. 6 for R. The error bar used in fitting $Q(z)$ was not $\sigma(Q)$ but the fitting error of the Q peak. The fitting error, which corresponds to the increase of 1.0 in the chi-squares, was usually small lying in the data points. The error bars attached to the FWHM and $\sigma(z)$ data points correspond to the fitting errors of the $A1+A2$ peak width and $\sigma(R)$, respectively.

with $\lambda_a\sim$122 mm for $A1$ and 129 mm for $A2$. The z-dependences of $A1$ and $A2$ are similar to each other, indicating the approximate uniformity of the strip along the length with respect to the emission intensity and attenuation. While the sum of $A1+A2$ could be fit well with the sum of two exponentials

$$f_{sum}(z)=\text{const.}[\exp(z/\lambda_a)+\exp(-z/\lambda_a)] \quad (2)$$

this function is poorly sensitive to λ_a. Then, instead of fitting, the solid curve on the $A1+A2$ data is simply drawn with $f_{\rm sum}(z)$ by

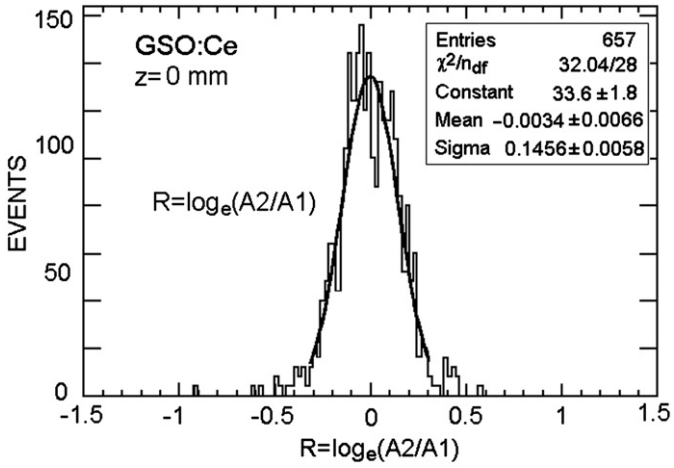

Fig. 6. A typical spectrum of R for total absorption events in GSO:Ce at the injection position z=0. The solid curve gives a Gaussian fit. The triggering condition is the same as in Fig. 4.

substituting λ_a with 129 mm obtained in the fit of $A2$. The agreement between $f_{\rm sum}(z)$ with data is visibly good as expected. The situation is the same for $\Delta E/E$, which is given by the ratio of the FWHM width of $A1+A2$ to $A1+A2$. If we assume that $\Delta E/E$ should be dominated by the statistical fluctuation of LY, it should have a z dependence of

$$f_{res}(z)=\text{const.}[\exp(z/\lambda_a)+\exp(-z/\lambda_a)]^{-1/2}. \quad (3)$$

Since this function is not sensitive to λ_a, the solid curve on the $\Delta E/E$ data is simply drawn with $f_{\rm res}(z)$ by substituting in it a fixed λ_a of 129 mm again. The agreement between $f_{\rm res}(z)$ with data is visibly good again as expected.

The injection position z of γ-rays can be obtained by comparing the pulse heights of $A1$ and $A2$. We can define for each event

$$R=\log_e(A2/A1). \quad (4)$$

A typical spectrum of R is presented in Fig. 6 for events in the total absorption peak. Since the separation between the total absorption peak and the Compton tail was always good (see Fig. 4), the cut between them was straightforward in any of the pulse height spectra of $A1$, $A2$, and $A1+A2$. The spectrum of R obtained in each run for a fixed injection position z showed a sharp peak as seen in Fig. 6. The peak was fit with a single Gaussian to obtain its mean $R(z)$ and width $\sigma(R)$. The $R(z)$ is plotted versus z in Fig. 5b with $\sigma(R)$ as its error bar. Substituting Eq. (1) into Eq. (4), we have the following approximate relation:

$$R(z)=2z/\lambda_a. \quad (5)$$

Actually the $R(z)$ spectrum can be fit well with a straight line Eq. (5) with λ_a=129 mm, which is consistent with 129 and 122 mm obtained in the fit of $A2$ and $A1$, respectively. Eq. (5) gives the position resolution $\sigma(z)$ as

$$\sigma(z)=\lambda_a\sigma(R)/2. \quad (6)$$

Then, from λ_a=129 mm and $\sigma(R)$ as shown in Fig. 6, we obtain $\sigma(z)\sim$8.9 mm almost independently of z (Fig. 5c). Here, we note that $\sigma(R)$ can be written as

$$\sigma(R)=\{[\sigma(A1)/A1]^2+[\sigma(A2)/A2]^2\}^{1/2}. \quad (7)$$

This gives a relation of $\sigma(R)\sim 2\sigma(A1+A2)/(A1+A2)$ for the injection at z=0, where $A1\sim A2$ holds. Actually for GSO:Ce at z=0, we obtained $\sigma(R)$=0.146 in Fig. 6, and $2\sigma(A1+A2)/(A1+A2)\sim$0.148 in Fig.4a.

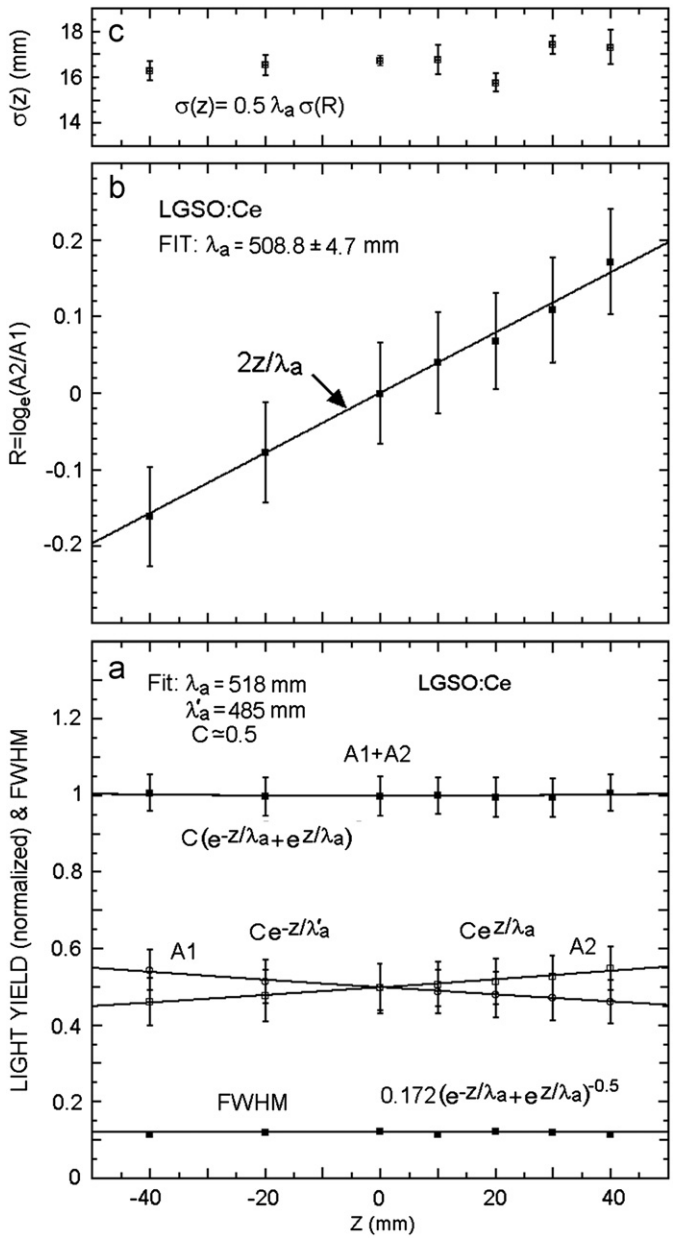

Fig. 7. Obtained result in LGSO:Ce for 0.511 MeV γ-rays. See Section 2.2 for the triggering condition and the captions of Fig. 5 for quantities. (a) Pulse heights $A1$, $A2$, sum of $A1+A2$ and FWHM of the $A1+A2$ versus z. (b) R and (c) $\sigma(z)$. Solid curves give the fit. In the fit for $A1+A2$ and FWHM, only the overall constant was taken as a fitting parameter by fixing λ_a at 500 mm (see text). For the error bars attached to data points, see the captions for Fig. 5.

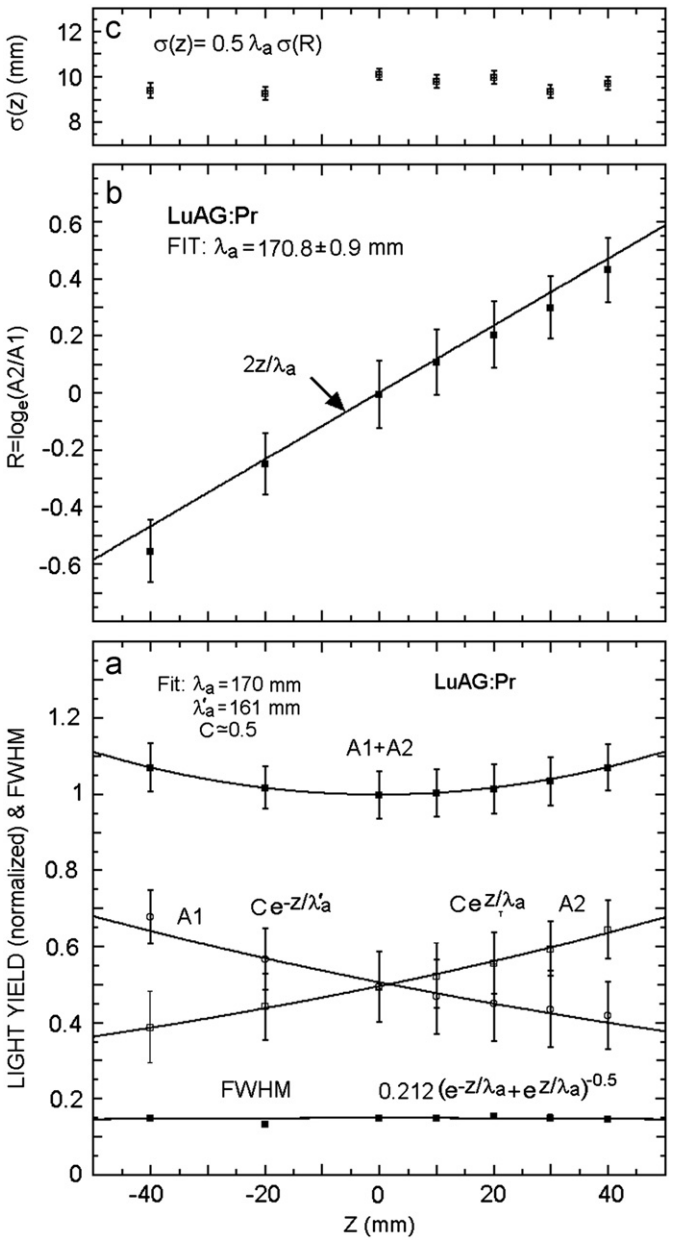

Fig. 8. Obtained result in LuAG:Pr for 0.511 MeV γ-rays. See Section 2.2 for the triggering condition and the captions of Fig. 5 for quantities. (a) Pulse heights $A1$, $A2$, sum of $A1+A2$ and FWHM of the $A1+A2$ versus z. (b) R and (c) $\sigma(z)$. Solid curves give the fit. In the fit for $A1+A2$ and FWHM, only the overall constant was taken as a fitting parameter by fixing λ_a at 170 mm (see text). For the error bars attached to data points, see the captions for Fig. 5.

While the asymmetry parameter $A=(A2-A1)/(A2+A1)$ [1] should be similarly useful as R to obtain $\sigma(z)$, R is more convenient since it gives a simple expression of Eq. (6) for $\sigma(z)$.

3.2. LGSO:Ce

Data analysis was similar to GSO:Ce. A typical pulse height spectrum of the sum of $A1$ and $A2$ for $z=0$ is given in Fig. 4. The LY was 4.63 times GSO:Ce at $z=0$ from comparison of the total absorption peak position.

Fig. 7a gives the z-dependences of the $A1$, $A2$, $A1+A2$ and $\Delta E/E$. The dependence of $A2$ (or $A1$) on z can be fit well with Eq. (1) with $\lambda_a \sim 518$ mm (or 485 mm). The z-dependences of $A1$ and $A2$ are similar to each other, indicating the approximate uniformity of the strip with respect to the emission intensity and attenuation. Due to the same reason as mentioned for GSO:Ce, $A1+A2$ and $\Delta E/E$ are poorly sensitive to λ_a. Instead of fitting, therefore, the solid curves on the $A1+A2$ and $\Delta E/E$ data in Fig. 7a are simply drawn with $f_{sum}(z)$ of Eq. (2) and $f_{res}(z)$ of Eq. (3), respectively, by substituting $\lambda_a=500$ mm, an average value obtained in the fit of $A1$ and $A2$.

The injection position z can be obtained from R of Eq. (4). The spectrum of R for the events in the total absorption peak in each run for a fixed z showed a single peak similar to Fig. 6. The peak was fit well with a single Gaussian to obtain $R(z)$ and $\sigma(R)$. The obtained $R(z)$ is plotted versus z in Fig.7b with $\sigma(R)$ as its error bar. Based on Eq. (5), $R(z)$ was fit well with $2z/\lambda_a$ with $\lambda_a=509$ mm, which is consistent with 518 and 485 mm obtained

in the fit of $A2$ and $A1$, respectively. From the obtained λ_a and $\sigma(R)$, the position resolution $\sigma(z)$ is given by Eq. (6) to be 16.8 mm almost independently of z (Fig. 7c).

3.3. LuAG:Pr

Data analysis was again similar to GSO:Ce. The LY was 1.82 times GSO:Ce from Fig. 4. Fig. 8a gives the z-dependences of the $A1$, $A2$, $A1+A2$ and $\Delta E/E$. The z-dependence of $A2$ (or $A1$) can be well fit with a single exponential of Eq. (1) with $\lambda_a \sim 170$ mm (or 161 mm), indicating the approximate uniformity of the strip with respect to the scintillation intensity and attenuation. Since $A1+A2$ and $\Delta E/E$ are poorly sensitive to λ_a, fitting was not done. The solid curves on the data points were calculated from $f_{\mathrm{sum}}(z)$ of Eq. (2) and $f_{\mathrm{res}}(z)$ of Eq.(3), respectively, by substituting the typical value of $\lambda_a = 170$ mm obtained in the fit of $A2$.

To calculate the position resolution $\sigma(z)$, the spectrum of R for the total absorption events was first fit with a single Gaussian to obtain its mean $R(z)$ and the width $\sigma(R)$. If the z-dependence (Fig. 8b) of the obtained $R(z)$ and its error bar $\sigma(R)$ was fit with Eq. (5), we obtained $\lambda_a = 171$ mm, which was close to 170 and 161 mm obtained in the fit of $A2$ and $A1$, respectively. Substituting the obtained λ_a and $\sigma(R)$ into Eq. (6), we obtained $\sigma(z) \sim 10.0$ mm almost independently of z (Fig. 8c).

3.4. Resolution $\sigma(z)$ in timing difference method

We measured the $T1$(stop)$-T2$(start) spectra similarly as in our previous work [1]. While the obtained result was qualitatively similar to Ref. [1], the timing resolution $\sigma(T1-T2)$ was much smaller in the present work as shown in Fig. 9. For GSO:Ce, this improvement should come from the significantly larger LY registered in PMTs due to shorter strip length of 100 mm instead of 200 mm in Ref. [1]. For LGSO:Ce and LuAG:Pr, not only larger LY than GSO:Ce but also faster rise and decay should improve the timing resolution.

As a typical example, $T1-T2$ spectra in LGSO:Ce are compared in Fig. 9b for γ-ray injection at $z=-40$, 0 and $+40$ mm. We obtained $\sigma(T1-T2)$ of 0.25 ns rms almost independently of z between -40 and $+40$ mm. The timing resolution between two LSO:Ce crystals was reported to be 0.207 ns rms for the crystal of $3\times3\times30$ mm^3 [30] and 0.191 ns rms for $3\times3\times20$ mm^3 [18]. Compared with these results, the obtained resolution of 0.25 ns rms for the LGSO:Ce strip should be good if the following two differences are taken into account: first, the crystal is much longer, and second, the LY in each PMT was smaller by half due to the readout at both ends of the strip.

The $T1$ and $T2$ can be written as

$$\begin{cases} T1 = (0.5L+z)/c_{eff} + t1 \\ T2 = (0.5L-z)/c_{eff} + t2 \end{cases} \quad (8)$$

where $L=100$ mm is the strip length, z is the injection position (Fig. 3), and c_{eff} the effective light velocity along the z-axis. The additional delays $t1$ and $t2$ should depend on the scintillators and PMT. The delay due to the mean transit time of PMT should be approximately canceled out in $T1-T2$. The transit time spread of PMT is independent of scintillator and z, and may be included in the measuring errors of both $T1$ and $T2$.

The c_{eff}^{-1} terms in Eq. (8) should originally come from the geometry and refractive index of the strip, being independent of the scintillation characteristics of the crystal. On the contrary, the $t1$ and $t2$ depend on the scintillation LY as well as the rise and decay times. They should be actually determined by the time elapsed before the occurrence of the first phe in the PMT. The first phe is important because the discriminator thresholds were set slightly below the single phe level. For simplicity we will here ignore $t1$ and $t2$ and discuss their effects later in Section 4.3. Neglect of $t1$ and $t2$ means that their effects should be effectively

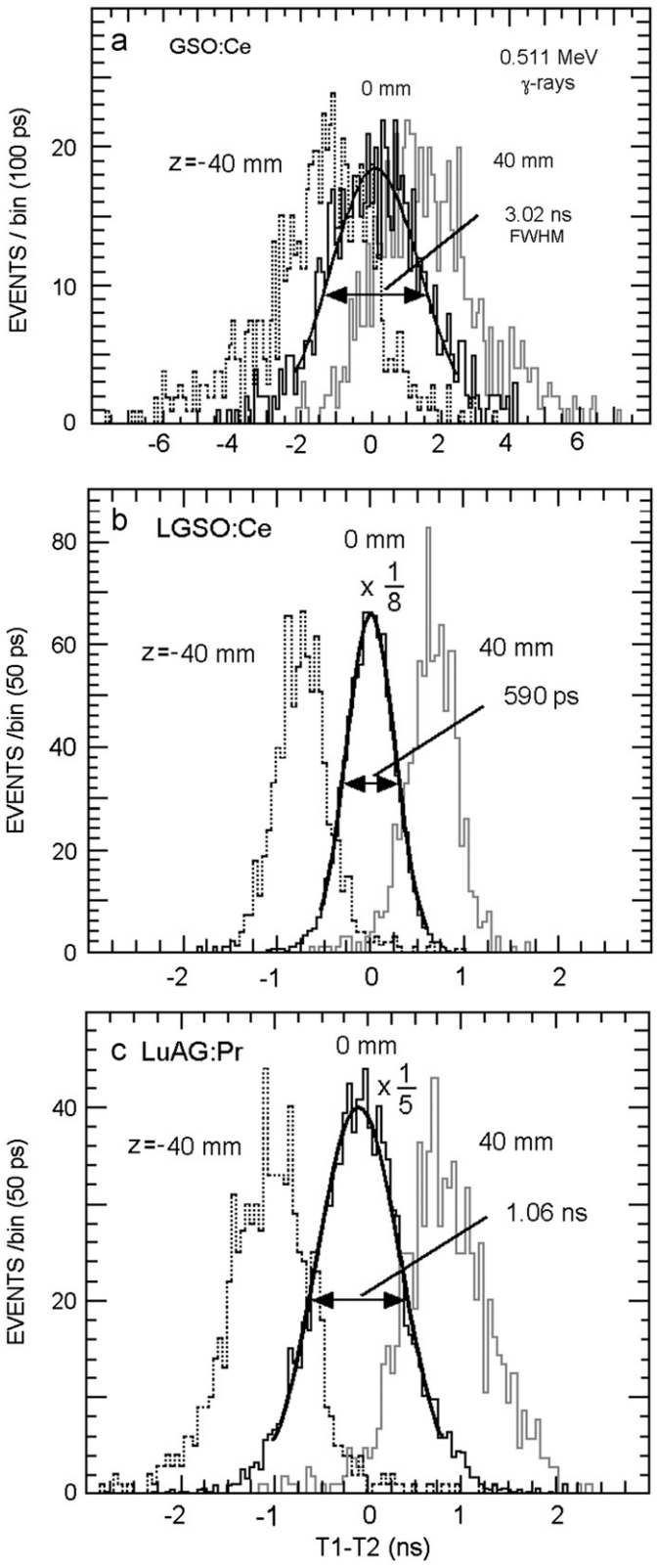

Fig. 9. Typical spectra of the timing difference between $T2$ (start) and $T1$ (stop) in (a) GSO:Ce, (b) LGSO:Ce and (c) LuAG:Pr for γ-ray injection at $z=-40$, 0 and 40 mm. The zero of $T1-T2$ is set arbitrarily. A Gaussian fit is shown with solid curves only for $z=0$. The spectra are left and right symmetric for $z=0$, while some asymmetries exist for $z=-40$ and $+40$ mm.

Table 3
Comparison of the effective light velocity $c_{\rm eff}$ and timing resolution $\sigma(T1–T2)$ at $z=0$ for different scintillator strips.

Scintillator strip	GSO:Ce	LGSO:Ce	LuAG:Pr	GSO:Ce[1]
Size, mm^3	$2\times2\times100$	$2\times2\times100$	$2\times2\times100$	$2\times2\times200$
$c_{\rm eff}$, cm/ns	6.54	11.4	8.54	3.0
$\sigma(T1-T2)$ at $z=0$, ns	1.28	0.25	0.45	2.12
$\sigma(z)$, mm	42	14.3	19.2	32

included in $c_{\rm eff}$, making $c_{\rm eff}$ depend not only on the LY but also on the rise and decay times. Under this approximation, Eq. (8) is reduced to the following simple relation:

$$z=0.5c_{eff}(T1-T2). \quad (9)$$

From Fig. 9b, we see that the peak position shifts by 1.4 ns as z changes by 80 mm in the LGSO:Ce strip. Eq. (9) then gives $c_{\rm eff}=11.4$ cm/ns. The position resolution is derived from Eq. (9) as

$$\sigma(z)=0.5c_{eff}\sigma(T1-T2). \quad (10)$$

Substitution of $c_{\rm eff}=11.4$ cm/ns and $\sigma(T1-T2)=0.25$ ns at $z=0$ obtained already into Eq. (10) gives $\sigma(z)=14.3$ mm at $z=0$ (Table 3).

The quantities $c_{\rm eff}$, $\sigma(T1-T2)$, and $\sigma(z)$ for GSO:Ce and LuAG:Pr strips were obtained in the similar way as for LGSO:Ce, and compared in Table 3; $\sigma(z)$ was 40 and 19.2 mm in GSO:Ce and LuAG:Pr, respectively. The $c_{\rm eff}=6.54$ for GSO:Ce and 8.54 cm/ns for LuAG:Pr are significantly less than 11.4 cm/ns for LGSO:Ce, as expected from the smaller LY and/or slower rise and decay.

4. Discussions

4.1. Effective light attenuation length λ_a

The obtained λ_a of 509 mm for LGSO:Ce was much longer than 128 mm for GSO:Ce and 171 mm for LuAG:Pr (Table 2). We have not expected this since the overlap between the excitation and emission peaks in LGSO:Ce is similarly large as in GSO:Ce (Fig. 2), suggesting possible significant self-absorption. The obtained result may indicate that the internal transparency and/or total reflection on the walls may be much better in LGSO:Ce than GSO:Ce. According to Dr. Ishibashi [31], the internal attenuation length of LGSO:Ce was as large as 300 cm at 420 nm in the best samples. To our measurement the corresponding quantity of GSO:Ce 1.5 mol% was around 30 cm at 450 nm in a typical crystal of $2\times2\times20$ cm^3.

Another result to be noted is that the λ_a of 128 mm in the 100 mm long GSO:Ce strip was roughly twice as large as that of 67 mm [1] in the 200 mm long one with the same cross-section of 2×2 mm^2. Both strips were cut from the same large ingot. The length/width (or thickness) ratio, called the aspect ratio [1], is 50 or 100 in them. If the aspect ratio is much larger than typically 10, direct photons from the γ-ray injection point ($z=0$) to PMT would give only a small contribution to the PMT pulse height due to small solid angle, making the contribution of the photons which experienced total reflection on the strip walls much more important. Then we can approximate that λ_a should be determined by internal attenuation and incomplete total reflection on the walls, and that the light reflected back from the PMT window as well as from the strip surfaces could be ignored. Under these approximations, λ_a should hardly depend on the strip length, because the light transmission from the γ-ray injection point to the PMT becomes essentially one directional. The λ_a should be locally the same anywhere in the strip. The increase in λ_a for shorter strips may be due to any of the three quantities which are neglected in the above approximation: (1) the light reflected back from the other end of strip, (2) the reflected light from the strip surfaces due to incomplete total reflection, (3) the reflected light from the strip surfaces for the injection angles outside the total reflection.

While we estimated each contribution, we cannot explain the large difference of λ_a between the two strip lengths. We still need to fully understand the mechanism for the significant dependence of λ_a on the strip length at the present stage. To further understand the roles of internal attenuation and the times of total reflection, comparison of two 100 mm long GSO:Ce strips with the same cross-section area but different sizes of 2×2 mm^2 (the present sample) and 1×4 mm^2 (another sample cut from the same large ingot) is under way.

4.2. Light yield LY and energy resolution $\Delta E/E$

The LY ratios of the three scintillator strips of GSO:Ce:LGSO:Ce:LuAg:Pr were 1:4.63:1.82 from the 0.511 MeV γ-ray peak positions in Fig. 4. To estimate the LY in number of photoelectrons (phe), we measured the single phe peak for both PMTs *A*1 and *A*2 at all the HVs (700, 720 and 750 V) in the same setup as in the data taking. Removing the scintillator strip, laser light (410 nm, 33 ps duration) was injected at a constant rate to the PMT through a pinhole prepared in front of the window. A neutral density optical filter was inserted until the single phe peak was identified. Since the single phe peak was most clearly identified at the highest voltage 750 V which was applied for GSO:Ce, we first calculated the LY of GSO:Ce in phe, and then for the other scintillators by using the LY ratios given in the beginning of the present section. The LYs of GSO:Ce, LGSO:Ce, and LuAG:Pr at $z=0$ were 380, 1758 and 691 phe/MeV, respectively (Table 2).

We compared the obtained LY in phe/MeV with expectation. The LY at $z=0$ can be given by a product of the nominal LY of scintillator $(\rm LY)_0$ in phe/MeV and four efficiencies [1]: (1) attenuation of photons through 50 mm transmission along the length due to internal absorption and incomplete total reflection on the walls, (2) geometrical efficiency $f_{\rm geo}$ for the light transportation from the source ($z=0$) to the strip end and refraction into PMT window under an assumption that total reflection on the walls should be complete, (3) $(\rm QE)_{av}=$QE of PMT averaged for the emission spectrum of scintillator, and (4) $f_{\rm gate}=$fraction of LY within the ADC gate width $t_{\rm gate}=300$ ns to the total one. Then we obtain the following relation:

$$LY(\text{in phe/MeV})=(LY)_0\exp(-50\ \text{mm}/\lambda_a)f_{geo}(QE)_{av}f_{gate}. \quad (11)$$

The parameters are listed in Table 4. $(\rm LY)_0$ and λ_a were taken from Tables 1 and 2, respectively. $f_{\rm geo}=0.19$ for GSO:Ce based on a Monte Carlo calculation [1]. The corresponding value of 0.196 for LGSO:Ce and 0.158 for LuAG:Pr was calculated in the similar way as for GSO:Ce. $(QE)_{av}$ was calculated by folding the nominal QE of PMT supplied by its manufacturer with the radioluminescence spectrum (Fig. 1). $f_{\rm gate}$ should be close to unity for LGSO:Ce, whose decay ($\tau=40$ ns) is much faster than $t_{\rm gate}=300$ ns. For GSO:Ce 1.5 mol%, the decay of two components listed in Table 1 gives $f_{\rm gate}$ of 96%. For LuAG:Pr, the decay process is more complicated. According to our measurement, fast components consist of

Table 4
Comparison of estimated and measured LY (see text).

Crystal	$(\rm LY)_0$, phe/MeV	λ_a mm	$f_{\rm att}$	$f_{\rm geo}$	$(\rm QE)_{av}$	$f_{\rm gate}$	LY phe/MeV	
							pred.	meas.
GSO:Ce	8000 [1]	128	0.6766	0.190	0.31	0.96	306	380
LGSO:Ce	23,000	509	0.9064	0.196	0.34	~1	1390	1758
LuAG:Pr	18,000	171	0.7465	0.158	0.39	0.78	646	691

$\tau_1=17$ ns for 35%, $\tau_2=119$ ns for 14%, and $\tau_3=1633$ ns for 51%. Much slower components, including $\tau_4=9000$ ns [21] and phosphorescence observed with $\tau_5=0.2$ ms, are not useful and have to be suppressed electronically for most of applications. We take useful fast component to be about 18,000 phe/MeV for $t_{gate}=1$ μs (Table 1) based on our measurement result of three times $Bi_4Ge_3O_{12}$ (BGO). Since 72.4% and 56.4% of the fast components (τ_1–τ_3) lie within 1 μs and 300 ns, respectively, we can take $f_{gate}=56.4\%/72.4\%=0.78$ for $(LY)_0=18{,}000$ phe/MeV (see Table 4).

The LY given by Eq. (11) is compared in Table 4 with the experimental result. The predicted values are by 10–20% smaller. The difference may be partly due to the ambiguity of ~10% in the $(LY)_0$. It may also be due to the contribution of the light reflected back from the other end of the strip, as mentioned in the previous section. Should this contribution be finite, it would increase f_{geo} in Eq. (11).

The FWHM energy resolution $\Delta E/E$ of 0.511 MeV γ-rays injected at $z=0$ was 17.7% in GSO:Ce, 12.2% in LGSO:Ce and 15.0% in LuAG:Pr (see Table 2). If the resolution is due only to the statistical origin, the obtained LY in Table 2 gives FWHM resolution of 16.9% in GSO:Ce, 7.86% in LGSO:Ce and 12.5% in LuAG:Pr. These numbers are a little smaller than the experimental resolutions, suggesting additional instrumental width of 5–9% FWHM.

For GSO:Ce, we can compare the present result for 100 mm long strip (LY=380 phe/MeV and $\Delta E/E=17.7\%$) with that for 200 mm long one (114 phe/MeV and 35%) [1]. The improvement of $\Delta E/E$ by $17.7\%/35\%=0.51$ times is almost consistent with the $(\text{LY ratio})^{-1/2}=(380/114)^{-1/2}=0.55$.

4.3. Position resolution $\sigma(z)$

$\sigma(z)$ was measured by two independent methods using pulse height ratio $A2/A1$ and timing difference $T1-T2$.

First, $\sigma(z)$ was obtained from $A2/A1$ according to Eq. (6). It was 8.9 mm rms in GSO:Ce, 16.8 mm in LGSO and 10.0 mm in LuAG:Pr at $z=0$ (see Table 2). LGSO:Ce with the largest LY gave the poorest resolution. This is because the large λ_a of 509 mm reduced the difference of $A2/A1$ from unity, thereby reducing its sensitivity to z.

The $\sigma(z)$ of GSO:Ce was improved from 10 mm in the $2\times2\times200$ mm^3 strip to 8.9 mm in the $2\times2\times100$ mm^3 one. This improvement in shorter strip should indicate that, referring to Eq. (6), the improving effect of the increased LY for $\sigma(R)$ outweighed the degrading effect of longer λ_a.

Second, $\sigma(z)$ obtained from $T1-T2$ according to Eq. (10) is compared in Table 2 with that from $A2/A1$. We see that $\sigma(z)$ from $T1-T2$ is poorer than that from $A2/A1$ except in LGSO:Ce. Eq. (10) shows that $\sigma(z)$ is given by half of the c_{eff} times $\sigma(T1-T2)$. We will below examine these two quantities:

(1) *Geometrical effects on c_{eff}*: Since the local light velocity is equal to c/n with c the light velocity in vacuum and n the refractive index of scintillator, the c_{eff} in Eq. (8) can be approximately given by dividing it by the ratio κ of the average light path length along zigzag motion to its projection on the z-axis. In the LGSO strip, the total reflection angle is 33.12° on the surface for $n=1.83$ (Table 1). For a rough estimation of κ, we make the following simplifications; the strip cross-section is circular, the light is emitted uniformly from a point on the z-axis at a distance ζ to PMT, and reaches the PMT window directly or after complete total reflection on the strip surface. Taking a phase space average within the cone of an opening angle of twice 56.88° (=90–33.12°), we obtain the average light path length of 1.332 ζ instead of ζ. Then we obtain $\kappa\sim1.332$ and $c_{eff}=c/(n\kappa)=0.41c=12.3$ cm/ns, which is not far from the experimental value of 11.4 cm/ns.

The situation is different for both GSO:Ce and LuAG:Pr. Similar estimation for GSO:Ce ($n=1.85$) gives $\kappa\sim1.339$ and $c_{eff}=0.40c=12.0$ cm/ns, which is significantly larger than the experimental value of 6.54 cm/ns. Estimation for LuAG:Pr ($n=1.99$) gives $\kappa\sim1.383$ and $c_{eff}=0.36c=10.9$ cm/ns, which is still sizably larger than the experimental value of 8.54 cm/ns. Smallness of the observed c_{eff} for GSO:Ce and LuAG:Pr may be attributed to the effects of the delays $t1$ and $t2$ in Eq. (8). Neglect of $t1$ and $t2$ in Eq. (9) must have resulted in reduction of c_{eff} when the LY is not large enough and/or the rise and decay time is not fast enough. This conjecture will be examined qualitatively in the following paragraphs.

(2) *Effects of the delays $t1$ and $t2$ on $T1-T2$ and c_{eff}*: As mentioned in Section 3.4, the $t1$ and $t2$ should represent the time elapsed before the occurrence of the first phe in the PMT. While they should occur within the rise time in many scintillators, no photoelectrons may be produced within the rise time if the scintillation LY and/or rise time should be too small. In such a case, the delays should occur in the decay time of the scintillation pulse. The delays should be small if the LY is sufficiently large and the rise time is small as in LGSO:Ce. Otherwise, the delays should become substantial as in GSO:Ce.

When the LY is not large enough and/or the rise and decay times are not fast enough, $T1-T2$ can be overestimated, then c_{eff} from Eq. (9) underestimated, and finally $\sigma(z)$ from Eq. (10) underestimated. To obtain an intuitive picture for the effects of LY and rise time on c_{eff}, we compare two injection points, one at the center ($z=0$), and the other close to $A2$ ($z=40$ mm). For the injection at $z=0$, $t1$ and $t2$, which give event by event fluctuations of $T1$ and $T2$, respectively, should be of the same level, keeping the mean of $T1$–$T2$ distribution unchanged. For the injection point at $z=40$ mm, the $A2$ pulse height should be increased while the $A1$ decreased. If the LY is small and the rise time is large, $t2$ should be decreased compared with $z=0$ advancing $T2$ (start), while $t1$ should be increased delaying $T1$ (stop). As the result, $T1-T2$ should be increased more than the geometrical contribution given by the c_{eff}^{-1} terms of the right-hand side of Eq. (8). Then, c_{eff} should be underestimated according to Eq. (9).

Since the light intensity registered in the PMT depends on z through light attenuation, $t1(t2)$ should also depend on z. Smaller LY and larger rise time tend to increase both $t1$ and $t2$, thereby increasing $T1-T2$ and $\sigma(T1-T2)$, and then decreasing c_{eff}. If we write the increase factor of $T1-T2$ by η, c_{eff} is reduced by η^{-1} according to Eq. (9). Since $\sigma(T1-T2)$ should be increased by a factor $\eta^{1/2}$, that comes from the fluctuation of η, $\sigma(z)$ of Eq. (10) should be finally decreased by $\eta^{-1/2}$.

As an example, we compare 100 and 200 mm long GSO:Ce strips. Since the LY of the latter is as small as 30% of the former (Table 2), $T1-T2$ in the latter should be increased by a factor $\eta=6.54/3.0=2.18$ (Table 3), which is given by the inverse ratio of c_{eff} for the two strips. Then $\sigma(z)$ should be finally decreased by $\eta^{-1/2}=0.68$ times in the 200 mm long strip in rough agreement with the experimental result of 32 mm/42 mm=0.76 times (Table 3).

4.4. Application of single crystalline scintillator strips or fibers

Among the three crystals evaluated, LGSO:Ce gave the largest LY, the best $\Delta E/E$, the longest λ_a and the poorest $\sigma(z)$. GSO:Ce gave the smallest LY, the poorest $\Delta E/E$, the shortest λ_a and the best $\sigma(z)$, while LuAG:Pr was in between. The cost of raw materials may be the lowest for GSO:Ce.

For the applications in particle physics experiments, choice of optimum crystals should depend on the requirements of specific particle detectors, since the characteristics of scintillator strips depend not only on the material but also on the length, cross-section and surface texture. The length should be one of the most

important factors which determine the obtainable $\Delta E/E$ and $\sigma(z)$, while the cross-section should limit the lateral position resolution. Choice of scintillators may be various since the scintillator size is of wide variety depending on the detectors.

For the applications to axial PET scanners, however, the scintillator size should not have large variety; the cross-section of strip will be within 1–10 mm^2, and the length within 10–30 cm. Both energy and position resolutions should be the most important. Then optimum scintillators could be chosen once the geometries of the PET scanners are defined. To compete with conventional human PET scanners using BGO, $\Delta E/E$ as small as 25% and $\sigma(z)$ as small as or smaller than 10 mm should be considered [1]. All the strips of GSO:Ce, LGSO:Ce and LuAG:Pr studied in the present work satisfy the requirements mentioned above, and appear promising (Table 2).

If the longitudinal position z of injected γ-rays should be measured only from the pulse height ratio at both ends so as to simplify the electronics, only LGSO:Ce fails to satisfy the requirement of $\sigma(z)<10$ mm, while the $\Delta E/E$ is by far better than 25% (see Table 2). Since the poor $\sigma(z)$ is due to too long λ_a, $\sigma(z)$ may be improved by reducing λ_a at a cost of degrading the LY and $\Delta E/E$. For example, we may reduce λ_a by half to 255 mm by appropriate surface treatment or reflector wrapping [6]. Then the LY for the γ-ray injection at $z=0$ should decrease to 1584 phe/MeV by a factor of $k=\exp(-50/509)=0.906$, and $\Delta E/E$ increase to 12.8% FWHM by $k^{-0.5}=1.05$. Then, $\sigma(R)$, which should be approximately proportional to $\Delta E/E$, is increased again by a factor of 1.05. As the result, $\sigma(z)$ of Eq. (6) would be improved from 16.8 to 8.82 mm.

If we consider $2\times2\times200$ mm^3 strips for the PET scanners with the axial length of 200 mm, GSO:Ce was found to be marginal due to $\Delta E/E$ as large as 35% [1]. For LGSO:Ce and LuAG:Pr, we assume that λ_a should decrease to half of the $2\times2\times100$ mm strips similarly as in GSO:Ce. Then the LY for γ-rays injected at the center $z=0$ can be estimated in the similar way as above. As the result, we can predict $\Delta E/E=14.1\%$ and $\sigma(z)=9.7$ mm for LGSO:Ce, and $\Delta E/E=23.2\%$ and $\sigma(z)=7.7$ mm for LuAG:Pr. This indicates that both LGSO:Ce and LuAG:Pr should be promising candidates.

LYSO:Ce and LGSO:Ce have similar physical as well as scintillation properties to each other (see Table 1). Promising properties were reported for LYSO:Ce strips with $3.2\times3.2\times100$ mm^3 [6]; for 0.511 MeV γ-rays injected to the centre ($z=0$), the λ_a was 420 mm, the LY 1173 phe/MeV, $\Delta E/E$ 14.6% FWHM, and $\sigma(z)$ 14.4 mm. The present result on LGSO:Ce with $2\times2\times100$ m^3 gave similar, or even better result; λ_a was 500 mm, LY 1758 phe/MeV, $\Delta E/E$ 12.2% FWHM and $\sigma(z)$ 10.9 mm (Table 2).

Axial PET scanners have not yet been realized. One of the reasons may be the difficulty in producing high-quality single crystalline scintillator fibers at a reasonable cost in spite of many progresses achieved [2]. Further progress is waited for producing fibers having as high quality as bulk single crystals with a cross-section of a few mm square and a length as large as 100-300 mm.

5. Conclusion

The obtained result can be summarized as follows:

(1) We compared $2\times2\times100$ mm^3 strips of GSO:Ce 1.5 mol%, LGSO:Ce 0.15 mol% and LuAG:Pr 2.5 mol% for 0.511 MeV γ-rays. The z dependences of LY at each end can be fit well by a single exponential $\exp(z/\lambda_a)$ with $\lambda_a\sim128$, 509 and 171 mm for GSO:Ce, LGSO:Ce, and LuAG:Pr, respectively.

(2) Sum of the pulse height at both ends for the γ-ray injection at $z=0$ gave (LY, $\Delta E/E$ in FWHM)=(380 phe/MeV, 17.7%), (1758 phe/MeV, 12.2%), and (691 phe/MeV, 15.0%) in GSO:Ce, LGSO:Ce and LuAG:Pr, respectively.

(3) $\sigma(z)$ of the injection position z obtained from the pulse height ratio at both ends was 8.9, 16.8, and 10.0 mm rms in GSO:Ce, LGSO:Ce and LuAG:Pr, respectively. While z was also measured from the timing difference at both ends, comparable or even smaller $\sigma(z)$ (14.3 mm) was obtained only in LGSO:Ce, which has large LY and fast rise time.

(4) To obtain good $\Delta E/E$ and $\sigma(z)$ at the same time, large LY, fast rise time, and moderately large λ_a are important for scintillator strips. All the tested crystals appear promising depending on their applications in fine-segmented particle detectors as well as axial PET scanners.

(5) The λ_a in the 100 mm long GSO:Ce strip was twice as large as that in the 200 mm long one with the same cross-section.

Acknowledgments

The authors would like to express sincere thanks to Dr. H. Ishibashi of Hitachi Chem. Co. for carefully preparing the thin and long GSO:Ce and LGSO:Ce single crystals of high quality.

This work was supported in part by the Science Research Promotion Fund from the Promotion and Mutual Aid Corporation for Private Schools of Japan, a grant from Research Institute of Advanced Science and Technology, Kyoto-Sangyo University, and the Ministry of Education, Culture, Sports, Science and Technology of Japan under Grant-in-Aid for Scientific Research.

References

[1] S. Aogaki, et al., Nuclear Instruments and Methods in Physics Research Section A 614 (2010) 250.
[2] C. Pedrini, C. Dujardin, Crystal fibers and thin films for imaging applications, in: Radiation Detectors for Medical Applications, S. Tavernier, et al., (Eds.), Springer, The Netherlands, 2006, p. 275.
[3] P. Lecoq, Journal of Physics: Conference Series 160 (2009) 012016.
[4] P. Anfre, et al., IEEE Transactions on Nuclear Science NS-54 (2007) 391.
[5] A. Braem, et al., Nuclear Instruments and Methods in Physics Research Section A 610 (2009) 192.
[6] A. Braem, et al., Nuclear Instruments and Methods in Physics Research Section A 571 (2007) 419.
[7] H. Ishibashi, et al., IEEE Transactions on Nuclear Science NS-36 (1989) 170.
[8] C.L. Melcher et al., in: Proceedings of the Third International Conference on Inorganic Scintillators and their Applications (SCINT95), Delft, 1995, p. 309.
[9] M. Kobayashi, S. Kobayashi, Nuclear Physics A586 (1995) 457.
[10] T. Takahashi, et al., Astronomy and Astrophysics Supplement Series 120 (1996) 645.
[11] G. Tarantola, et al., Journal of Nuclear Medicine 44 (2003) 756.
[12] C.L. Melcher, et al., Current and future use of LSO:Ce scintillators in PET, in: S. Tavernier, et al., (Eds.), Radiation Detectors for Medical Applications, Springer, The Netherlands, 2006, p. 243.
[13] D.W. Cooke, et al., Journal of Applied Physics 88 (2000) 7360.
[14] S. Shimizu, et al., IEEE Transactions on Nuclear Science NS-53 (2006) 14.
[15] M. Moszynsky, et al., IEEE Transactions on Nuclear Science NS-54 (2007) 725.
[16] T. Usui, et al., IEEE Transactions on Nuclear Science NS-54 (2007) 19.
[17] M. Tanaka, et al., Nuclear Instruments and Methods in Physics Research Section A 404 (1998) 283.
[18] M. Kapusta, et al., IEEE Transactions on Nuclear Science NS-47 (2000) 1341.
[19] D.W. Cooke, et al., Journal of Luminescence 106 (2004) 125.
[20] K. Kamada, et al., IEEE Transactions on Nuclear Science NS-56 (2009) 570.
[21] L. Swiderski, et al., IEEE Transactions on Nuclear Science NS-56 (2009) 2499.
[22] I. Holl, et al., IEEE Transactions on Nuclear Science NS-35 (1988) 105.
[23] R. Mao, et al., IEEE Transactions on Nuclear Science NS-55 (2008) 2425.
[24] Y. Usuki (Furukawa Co.): A Private Communication on Measurement of Refractive Index of LuAG:Pr at 310 nm.
[25] D.P. Bortfeld, H. Meier, Journal of Applied Physics 43 (1972) 5110.
[26] Hamamatsu Photonics, UBA, SBA Photomultiplier Series, Technical Note, TPMH1305E03, 2008.
[27] H. Farhi, et al., Optical Materials 30 (2008) 1461.
[28] T. Yanagida, et al., Nuclear Instruments and Methods in Physics Research Section A 652 (2011) 256.
[29] S. Aogaki, F. Takeutchi, IEEE Transactions on Nuclear Science NS-57 (2010) 1502.
[30] W.W. Moses, et al., IEEE Transactions on Nuclear Science NS-46 (1999) 474.
[31] H. Ishibashi (Hitachi Chem. Co. Ltd.), A Private Communication.